# A tool for designing digital filters for the Hankel and Fourier transforms in potential, diffusive, and wavefield modeling

## ABSTRACT

The open-source code `fdesign` makes it possible to design digital linear filters for the Hankel and Fourier transforms used in potential-, diffusive-, and wavefield modeling. Digital filters can be derived for any electromagnetic method, such as methods in the diffusive limits (direct current, controlled-source electromagnetics) as well as methods using higher frequency content (ground-penetrating radar, acoustic and elastic wavefields). The direct matrix inversion method is used for the derivation of the filter values, and a brute-force inversion is carried out over the defined spacing and shifting values of the filter basis. Included or user-provided theoretical transform pairs are used for the inversion. Alternatively, one can provide layered subsurface models that will be computed with a precise quadrature method using the electromagnetic modeler `empymod` to generate numerical transform pairs. The comparison of the presented 201 pt filter with previously presented filters shows that it performs better for some standard controlled-source electromagnetic cases. The derivation of a longer 2001 pt filter for a ground-penetrating radar example with 250 MHz center frequency proves that the filter method works also for wave phenomena, not only for diffusive

electromagnetic fields. The presented algorithm provides a tool to create problem specific digital filters. Such purpose-built filters can be made shorter and can speed up consecutive potential-, diffusive-, and wavefield inversions.

## INTRODUCTION

In his Ph.D. thesis, Ghosh (1970) proposed a linear filter method for the numerical evaluation of Hankel transforms that subsequently revolutionized the computation of electromagnetic (EM) responses in the field of geophysical exploration. If you use a code that calculates EM responses in the wavenumber-frequency domain and transforms them to the space-frequency domain, chances are high that it uses the *digital linear filter* (DLF) method. Most practical 1D EM modeling codes rely on the DLF method for rapid computations; these codes are not only used for standalone simulations of EM fields in layered 1D media, but they are also commonly embedded within 3D modeling codes for computing the primary fields in scattered-field formulations or for the background fields required by integral equation methods. Thus, the DLF method is an important component of many commonly used modeling codes for EM geophysical data.

Ghosh (1971a) states that the DLF idea is based on suggestions made four decades earlier by Slichter (1933) and Pekeris (1940), in that "*the kernel function is dependent only on the layer parameters, and an expression relating it to the field measurements can be obtained by mathematical processes.*" However, until the introduction of DLF, these suggestions found no widespread use, likely because of the missing computer power to calculate the filter coefficients. He further states that credit goes to Koefoed (1968, 1970), who retook the task of direct interpretational methods with the introduction of raised kernel functions. DLF is, as such, an improvement of that approach, providing a faster and simpler method.

The DLF technique is sometimes referred to as the *fast Hankel transform* (FHT), popular because of the similarity of the name to the well known *fast Fourier transform* (FFT), although the algorithms for these techniques are completely different. The FHT name was

likely inspired by the title of a paper by Johansen and Sørensen (1979). However, the name FHT can be misleading as it has *Hankel* in the name, whereas the DLF approach can more generally be applied to other linear transforms, for example Fourier sine and cosine transforms.

The introduction of linear filters to EM geophysics, in parallel with rising computational power, initiated a wealth of investigations, leading to the development of computer programs that extended and improved the DLF method, and to numerous publications. These publications fall broadly into one or several of three categories: (1) new applications that extend the usage of DLF to other EM measurement techniques; (2) filter improvements that provide either new filters or improved methods for the determination of filter coefficients; and (3) computational tools that compute EM responses using DLF techniques. Here, we briefly review the most relevant publications, without claiming completeness.

*(1) New applications*

Ghosh used the method originally for the computation of type curves for Schlumberger and Wenner resistivity soundings: Ghosh (1971a) derives a resistivity model from given Schlumberger or Wenner sounding curves; and Ghosh (1971b) provides filters for the inverse operation, deriving resistivity sounding curves from a given resistivity model. The method was next applied to electromagnetic soundings with horizontal and perpendicular coils (Koefoed et al., 1972), to vertical coplanar coil systems (Verma and Koefoed, 1973), to dipoles and other two electrode systems (Das and Ghosh, 1974; Das et al., 1974; Das and Verma, 1980; Sørensen and Christensen, 1994), and to vertical dikes, hence vertical instead of horizontal layers (Niwas, 1975). The first filters were specific to a particular resistiv-

ity sounding type and its transform; later publications used the method to get one type curve from another type curve (Kumar and Das, 1977, 1978), or generalized the method to be applicable to a wider set of problems (Davis et al., 1980; Das and Verma, 1981b; Das, 1984; O'Neill and Merrick, 1984). Eventually, it passed from pure layered modeling to primary-secondary field formulations for 3D problems, where DLF is used to compute the spatial Fourier-Hankel transforms in a horizontally layered background medium and to compute transient responses from frequency domain computations (Das and Verma, 1981a, 1982; Anderson, 1984; Newman et al., 1986; Kruglyakov and Bloshanskaya, 2017). Other publications delved into the theory of the method, analyzing the oscillating behaviour of the filters and trying to estimate the error of DLF (Koefoed, 1972, 1976; Johansen and Sørensen, 1979; Christensen, 1990).

*(2) Filter improvements*

Ghosh (1970) derived the filter coefficients in the spectral domain by dividing the output spectrum by the input spectrum followed by an inverse Fourier transform. Improvements to the determination of filter coefficients were provided by O'Neill (1975); Nyman and Landisman (1977); Das (1982), or specifically for the Fourier transform by Nissen and Enmark (1986). A direct integration method was used by Bichara and Lakshmanan (1976) and Bernabini and Cardarelli (1978). Koefoed and Dirks (1979) proposed a Wiener-Hopf least-squares method, which was further improved by many authors (Guptasarma, 1982; Murakami and Uchida, 1982; Guptasarma and Singh, 1997). Kong (2007) proposed a direct matrix inversion method to solve the convolution equation, which requires only the input and output sample values. To evaluate the filter's effectiveness, he defines a good filter as one that recovers small or weak diffusive EM fields. This method was also used by Key

(2009, 2012) to create a suite of filters accurate for marine EM data. Most works have published filters for the Hankel transform with $J_0$ and $J_1$ Bessel functions (or $J_{-1/2}$, $J_{1/2}$ if applied to the Fourier sine/cosine transform), as all higher Bessel functions can be rewritten, via recurrence relations, using only use these two. Mohsen and Hashish (1994) is one of the rare cases which provides $J_2$ filter weights.

*(3) Computational tools*

The most well-known codes are likely Anderson's freely available ones. Anderson (1973) extends the method to transient responses, applying DLF not only to the Hankel transform, but also to the Fourier transform. A transient signal can therefore be obtained be applying twice a digital filter to the wavenumber-frequency domain calculation. Anderson (1975, 1979) presents improved filters for both Fourier and Hankel transforms, introducing measures to significantly speed-up the calculation, such as the lagged convolution or using the same abscissae for $J_0$ and $J_1$. Anderson (1982) and the included 801 pt filter became the de facto industry standard, to which subsequent filters were compared. Anderson (1989) presents a hybrid solution that uses either the DLF or a much slower but highly accurate adaptive-quadrature approach, which can also be used to measure the accuracy of the DLF. Key (2012) presented codes for comparing the DLF approach with a speed optimized quadrature method called quadrature-with-extrapolation (QWE); despite its optimizations, QWE is still not as fast as DLF, but it remains valuable as an independent tool for testing the accuracy of particular filters for the DLF method. Other examples include the codes by Johansen (1975), an interactive system for interpretation of resistivity soundings, and a tool to calculate filter coefficients by Christensen (1990). The latter is available upon request and was used, for instance, in all the open-source modeling and inversion routines

of CSIRO in the Amira Project 223 (Raiche et al., 2007).

All mentioned publications have in common that they were derived for direct current methods (DC) or low frequency methods, such as time-domain shallow EM methods (TEM), or controlled-source electromagnetics (CSEM), but not for high frequency methods such as ground-penetrating radar (GPR). Generally it was even thought that the filter method works only in the diffusive limit where the quasistatic approximation is valid (e.g., Hunziker et al., 2015). Nevertheless, Werthmüller (2017) tested DLF for modeling 250 MHz center-frequency GPR data using a 401 point filter that was designed for diffusive EM, and found that it was orders of magnitude faster than quadrature approaches. However, good quality results were only obtained for the first arrivals at short time-offsets and the later arrivals had poor quality. Yet, this promising initial test suggested it might be possible to specifically design a special filter for GPR frequencies where the EM fields propagate as waves rather than by diffusion.

While there are several versions of digital filters that are freely available, there are no open-source filter designing tools that readily available; they are either only described methods in articles or the codes are only available upon request by the author. Here, we address this gap by presenting the code `fdesign`, which is an open-source tool for designing general or purpose-built filters using the direct matrix inversion method. The code is completely open-source and can be run using freely available programming environments, thus there are few barriers to obtaining and running the code.

In the following sections we give a brief overview of the methodology, the theory, and the code, and then show examples of its usage, as well as presenting new filters for both CSEM and GPR data. The current article falls therefore into all three mentioned categories

7

by the new application of DLF to wave phenomena and by providing new filters with the accompanying code. The algorithm and many more examples of its usage can be found on github.com/empymod/article-fdesign. The examples can be used as templates to design new filters.

## METHODOLOGY

The algorithm `fdesign` is a filter designing tool using the direct matrix inversion method as described by Kong (2007) and based on scripts developed by Key (2012). The tool is an add-on to the EM modeler `empymod` (Werthmüller, 2017), written in Python, and hosted on GitHub, which should foster interaction and enable anyone to toy around, improve, and extend it. It can be used to derive digital linear filters for the Hankel and the Fourier transforms for potential, diffusive, and wavefield modeling (hence from DC to GPR).

Theoretically, it can be used to derive linear filters for any linear transform, as long as it is supplied with the inputs and outputs of a transform pair. Previous works have relied on using theoretical transform pairs commonly found in tables of integral transforms. Here we follow a similar approach, but we also propose a new method where filters could be derived from accurately computed numerical transform pairs, such as those computed using quadrature approaches. For example, the EM modeler `empymod` could be used to compute transform pairs for a particular class of model and data parameters (for example, a specific EM method and model of interest) using a slow but highly accurate quadrature method. A good filter derived from the resulting transform pairs could then be used for faster modeling of similar model and data parameters.

The main features of `fdesign` and some differences between it and the methods it is

based upon are:

- The algorithm computes many different filters for various spacing and shift values (brute-force), with an optional minimization routine for the best outcome of the brute-force step.

- Kong (2007) and Key (2012) optimize a filter for the $J_0$ filter, and then use the obtained shift and spacing value to calculate the $J_1$ values. The presented algorithm can optimize either $J_0$, $J_1$, or both in the optimization process. Five transform-pairs for each $J_0$ and $J_1$, and three transform pairs for each sine and cosine of often used functions are included in the routine, but any other transform pair can be provided as input.

- More complex or more specific numerical transform pairs can be provided instead of theoretical transform pairs by using the modeler `empymod`.

- Kong (2007) defines a *good* filter as one that recovers *weak* diffusive EM fields. In `fdesign`, you can define a relative error level that defines up to what error an obtained result is good or not. The optimization seeks to find the smallest amplitude field that is accurately modeled (i.e., minimizing the amplitude), but it has additionally another mode, where it will maximize the output abscissae $r$ of the transform pair instead of minimizing the amplitude. The two modes yield the same result in the general, simple case of fast decaying transform pairs. However, for some complex models and specifically for very high frequencies, maximizing $r$ will yield much better and more consistent results.

- The algorithm can solve under-, equal-, and over-determined linear systems.

- The real or the imaginary part can be used for the inversion of complex transform pairs.

The quality of a filter depends heavily on the model chosen for comparison. An obtained filter might be very good for one model or data acquisition setup, but not that good for another one, which is no different for this designing tool. There is no way to estimate the error of a result obtained with a certain filter if you apply it to any other model, unless you calculate this other model with another method for comparison. All results presented here should therefore be taken with a certain care. Further, when applying a new filter to a significantly different model and/or data space than what it has previously been tested on, we recommend first verifying its accuracy in that space by a comparison with results computed with a quadrature method such as QWE, which is also available in `empymod`.

**Theory**

Most of the articles mentioned in the review have detailed derivations of the digital filter method. In this article we focus on the algorithm, and summarize the theory only very briefly by following Key (2012). In electromagnetics we often have to evaluate integrals of the form

$$F(r) = \int_0^\infty f(l)K(lr)\mathrm{d}l \ , \tag{1}$$

where $l$ and $r$ denote input and output evaluation values, respectively, and $K$ is the kernel function. In the specific case of the Hankel transform $l$ corresponds to wavenumber, $r$ to offset, and $K$ to Bessel functions; in the case of the Fourier transform $l$ corresponds to frequency, $r$ to time, and $K$ to sine or cosine functions. In both cases it is an infinite integral which numerical integration is very time-consuming because of the slow decay of

the kernel function and its oscillatory behaviour.

By substituting $r = e^x$ and $l = e^{-y}$ we get

$$e^x F(e^x) = \int_{-\infty}^{\infty} f(e^{-y}) K(e^{x-y}) e^{x-y} \mathrm{d}y \ . \tag{2}$$

This can be re-written as a convolution integral and be approximated for an $N$-point filter by

$$F(r) \approx \sum_{n=1}^{N} \frac{f(b_n/r) h_n}{r} \ , \tag{3}$$

where $h$ is the digital linear filter, and the logarithmically spaced filter abscissae is a function of the spacing $\Delta$ and the shift $\delta$,

$$b_n = \exp\left\{\Delta(-\lfloor (N+1)/2 \rfloor + n) + \delta\right\} \ . \tag{4}$$

*Note to reviewers: In equation 4 $N/2$ changed to $\lfloor (N+1)/2 \rfloor$.* From equation 3 it can be seen that the filter method requires $N$ evaluations at each $r$. For example, to calculate the frequency domain result for 100 offsets with a 201 pt filter requires 20,100 evaluations in the wavenumber domain. This is why the DLF often uses interpolation to minimize the required evaluations, either for $F(r)$ in what is referred to as *lagged convolution DLF*, or for $f(l)$, which we here call *splined DLF*.

In the direct matrix inversion method for solving for the digital filter coefficients, equation 3 is cast as a linear system ~~as follows.~~*, where* $\Delta$ and $\delta$ are preassigned scalar values and $r$ is a range of $M$ preassigned values $r_m$. The filter base coefficients $b_n$ are computed using equation 4 and an array of values for $l$ are computed using $l_{mn} = b_n/r_m$. The linear system's left hand side (LHS) matrix $\mathbf{A}$ has dimensions $M \times N$ with coefficients ~~$A_{mn} = f(l_{mn})/r_n$~~$A_{mn} = f(l_{mn})/r_m$ and the right hand side (RHS) vector $\mathbf{v}$ has elements

11

~~$v_n = F(r_n)$~~ $v_m = F(r_m)$. The resulting linear system

$$\mathbf{A}\mathbf{h} = \mathbf{v} \tag{5}$$

can be solved by direct matrix inversion to obtain the vector of filter coefficients $\mathbf{h}$. For a given filter length $N$, there are many subjective choices that go into the practical implementation of this method, including the choice of the transform pairs $F(r)$ and $f(l)$, as well as the value for $M$ and the particular range and spacing of the values $r_m$. Once values are chosen for these variables, an optimal filter can be found by a grid search over $\Delta$ and $\delta$ for values that produce a high quality filter. The choice of metric for what constitutes a high quality filter is also subjective and is further discussed below.

**Pseudo-code for `fdesign`**

The main input variables are the filter length ($N$), the spacing ($\Delta$) and shift ($\delta$) ranges over which to loop, and the transform pairs for the inversion ($f_\mathrm{I}$) and the check of quality ($f_\mathrm{C}$). If $f_\mathrm{C}$ is not provided, then $f_\mathrm{I}$ is used for both. There are additional, optional input parameters, for instance to adjust how the RHS abscissae for the inversion $r_\mathrm{I} = p(b, N)$ are calculated, where $b$ is the filter base. Additionally, ranges $r$ for evaluating the check function need to be specified.

The basic steps are as follows:

1. Evaluate RHS of check-function $f_\mathrm{C}$:

   ~~$d_\mathrm{R} = f_\mathrm{C}.\mathrm{rhs}(r)$~~

   $d_\mathrm{R} = f_\mathrm{C}^{\mathrm{rhs}}(r)$

2. Loop over each value $\Delta_i$, $\delta_j$ (brute force*; parameters on the left-hand side are over-*

*written where i, j are not mentioned*):

(a) Calculate filter base:

~~$b_n = \exp\{\Delta_i(-N/2 + n) + \delta_j\}$~~

$b_n = \exp\{\Delta_i(-\lfloor(N+1)/2\rfloor + n) + \delta_j\}$

(b) Get required RHS and LHS evaluation points:

$r_{\mathrm{I}} = p(b, N)$

$l_{\mathrm{I}} = b/r_{\mathrm{I}}$

(c) Invert for filter coefficients:

~~$J_{ij} = \mathrm{solve}(f_{\mathrm{I}}.\mathrm{lhs}(l_{\mathrm{I}}), f_{\mathrm{I}}.\mathrm{rhs}(r_{\mathrm{I}}))$~~

$J = \mathrm{solve}\left[f_{\mathrm{I}}^{\mathrm{lhs}}(l_{\mathrm{I}}), f_{\mathrm{I}}^{\mathrm{rhs}}(r_{\mathrm{I}})\right]$

(d) Calculate numerically RHS of check-function $f_{\mathrm{C}}$ with current filter ~~$J_{ij}$~~$J$:

~~$d_{\mathrm{F}} = f_{\mathrm{C}}.\mathrm{lhs}(b/r) \cdot J_{ij} / r$~~

$d_{\mathrm{F}} = f_{\mathrm{C}}^{\mathrm{lhs}}(b/r) \cdot J / r$

(e) Store minimum recovered amplitude or maximum $r$ where relative error is less than the provided error:

$\chi_{ij} = g\left[\mathrm{argmin}\left(|(d_{\mathrm{F}} - d_{\mathrm{R}})/d_{\mathrm{R}}| > \mathrm{error}\right) - 1\right]$ , where $g$ is either $d_{\mathrm{R}}$ or $1/r$.

3. ~~Return filter~~ *Re-calculate (Steps 2a-2c) filter base and* coefficients which yield minimum amplitude or maximum $r$ (a local minimization can be run to polish the brute-force result):

$i_{\mathrm{best}}, j_{\mathrm{best}} = \mathrm{argmin}(\chi)$

*recalculate b, J with $i_{\mathrm{best}}, j_{\mathrm{best}}$*

~~return $J[\mathrm{argmin}(\chi)]$~~

4. *Return filter base and coefficients and error matrix (for visual QC):*

   *return b, J, χ*

**Minimization criteria**

Figure 1 shows the differences between the different minimization approaches; in (a) for a conventional, fast decaying transform pair; and in (b) for a more complex, high frequency layered model. The circles show the minimum amplitude used in previous approaches. This criterion is not ideal, as it is subject to some random fluctuations and depends on the choice of $r$. The squares show the minimum amplitude given a certain acceptable error, and the diamonds show the maximum $r$ given a certain acceptable error (the inversion is a minimization process, it therefore minimizes $1/r$, not $r$). In simple cases the minimum amplitude given an acceptable error and the maximum $r$ given an acceptable error will yield the same result. However, in complex cases the maximum $r$ is more consistent and therefore a much better criterion.

While the $\chi$ array is used to identify the optimal values of $\Delta$ and $\delta$, the value of $\mathrm{argmin}(\chi)$ will depend on the choice of the check function $f_C$ and can vary from one transform pair to another; thus it should not be used to compare the quality of filters created with different transform pairs.

## NUMERICAL EXAMPLES

The numerical examples are focused on the Hankel transform, although `fdesign` can be used to design digital linear filters for both Hankel and Fourier transforms. As there is no

difference in the procedure of the two, this should be sufficient to demonstrate the algorithm.

**Design**

Figure 2 shows the solution spaces of four consecutive inversion runs, where each run is a focus on a subsection of the previous run, indicated by the red square. The filter length in this case is $N = 201$, and the theoretical transform pairs are as given, e.g., in Anderson (1975):

$$\int_0^\infty l \exp\left(-al^2\right) J_0(rl)\, dl = \frac{\exp\left(\frac{-r^2}{4a}\right)}{2a} \; , \tag{6}$$

$$\int_0^\infty l^2 \exp\left(-al^2\right) J_1(rl)\, dl = \frac{r}{4a^2} \exp\left(-\frac{r^2}{4a}\right) \; , \tag{7}$$

where $a$ was set to 5. In the algorithm you can provide one pair for the inversion, and a different pair to get the minimum amplitude or the maximum $r$. In this case the same transform pair was used for both the inversion and the check of quality. The acceptable relative error was set to $1\%$. The RHS evaluation parameter for the inversion was set so that an over-determined system was evaluated with $M = 2N$ equations, where $r_\text{I}$ was logarithmically spaced from $\log_{10}(1/\max(b)) - 1$ to $\log_{10}(1/\min(b)) + 1$, where $b$ are the filter abscissae as given in equation 4. This is accomplished in `fdesign` by setting parameter $r_\text{def} = (1, 1, 2)$.

From the low resolution overview runs (a) and (b) it looks like this is a standard, straightforward minimization problem. However, from the more detailed results in (c) and (d) it becomes obvious that it is a minimization problem that has to be solved stochastically, as there are solutions with 2 orders of magnitude difference apparently randomly next to each other.

Figure 3 shows in (a) the filter values for $J_0$ and $J_1$ of the best 201 point filter obtained

15

this way, and in (b) its right-hand-side solution. The black dots indicate negative values, from which it can seen that adjacent values are often alternating between positive and negative contributions.

Designing filters is to a large extent trial and error. All input variables influence the outcome, and often a good filter is found by sheer luck of choosing the right starting parameters. Each of the input parameters has an effect on the outcome. It also depends heavily on the transform pairs $f_{\mathrm{I;C}}$; functions that decay rapidly are generally better, as noted by earlier authors (e.g. Anderson, 1975). It also depends on the filter length, and obviously heavily on the spacing and shift values. Another important point is how you define the right-hand evaluation points of the inversion ($r_{\mathrm{def}}$). Evaluating corresponding transform pairs separately or jointly also leads to different filter coefficients ($J_0$, $J_1$, or $J_0$ & $J_1$, or equally sine, cosine, or sine & cosine); also if the real or the imaginary part is used when complex transform pairs or `empymod` is used; and if it is inverted for the minimum amplitude or for the maximum $r$.

## CSEM

In this section we compare the 201 pt filter derived in the previous section to marine CSEM models used in Kong (2007), Key (2012), as well as for a land EM case.

Figure 4 compares the derived 201 pt filter with the two half-spaces case used by Kong (2007) in his Figure 5. The model consists of a $0.3125\,\Omega\,\mathrm{m}$ sea layer of infinite thickness above a subsurface $1\,\Omega\,\mathrm{m}$ half-space. The signal of a $1\,\mathrm{Hz}$ frequency $x$-directed electric source $50\,\mathrm{m}$ above the interface is measured at an $x$-directed electric receiver at the interface. In (a) it can be seen that the new 201 pt filter is able to recover smaller amplitudes than the

241 pt filter from Kong (2007), the 201 pt filter from Key (2012), and the 801 pt filter from Anderson (1982) (Wer201, Kong241, Key201, and And801, respectively). It behaves equally well as the quadrature with extrapolation (QWE), for which we used a 51 pt quadrature with relative and absolute tolerance of $10^{-12}$ and $10^{-30}$, respectively. The relative error is shown in (b), where the QWE result was taken as *truth*. For offsets greater than roughly 15.5 km the relative error becomes meaningless, as the QWE fails itself; this part is greyed out in the figure.

Figure 5(a) considers the canonical CSEM model as used in Key (2012) in his Figure 5: a $0.303\,\Omega\,\mathrm{m}$ sea with depth of 2 km, a background resistivity of $1\,\Omega\,\mathrm{m}$, in which a $100\,\Omega\,\mathrm{m}$ target layer of 100 m thickness is embedded at 1000 m below the seafloor. The source is located at 1990 m and receivers are positioned on the seafloor.

Figure 5(b) is a land case, with a background resistivity of $10\,\Omega\,\mathrm{m}$, in which a $500\,\Omega\,\mathrm{m}$ target of 100 m thickness is embedded at 1000 m below the surface. The source depth is 0.5 m and the receiver depth is 0.8 m. In both cases the new filter *Wer201* has generally a relative error which is orders of magnitude lower than the other filters. The relative error of the real part is given in black, whereas the relative error of the imaginary part is given in grey. It is interesting to note that the real and imaginary parts have very similar errors in *Wer201*, *Key201*, and *And801*, but that the imaginary part of *Kong241* seems to behave considerably better for most part than its real counterpart. To compare the real and the imaginary parts is insofar interesting as the digital filters are purely real valued.

It is very important to note again that other scenarios might yield very different error plots. Although the new 201 pt filter proves to be very accurate for these three models, it might not be the best filter in other cases. To verify the applicability of the filter we run

two different tests over a wide range of scenarios. Figure 6 shows the relative errors of DLF using the filter *Wer201* compared to QWE for a deep water model, a shallow water model, and a land model. The models consist of air (upper halfspace), a water layer in the first two examples, and a subsurface halfspace. Source depth is $1990\,\mathrm{m}$, $10\,\mathrm{m}$, and $0.5\,\mathrm{m}$ in the deep, shallow, and land case, respectively. Receiver depth is $2000\,\mathrm{m}$, $100\,\mathrm{m}$, and $0.8\,\mathrm{m}$. The subsurface halfspace resistivity varies from 1 to 10, 100, and $1000\,\Omega\,\mathrm{m}$ from the left to the right column. The error plots cover offsets from $50\,\mathrm{m}$ to $20\,\mathrm{km}$ on the x-axis, and $0.01\,\mathrm{Hz}$ to $10\,\mathrm{Hz}$ on the y-axis. It can be seen in the result that the filter is sufficiently precise for all practical CSEM cases, hence has generally an error far below $1\,\%$ $(10^{-2})$ in all cases. The exception are large offsets with relatively high frequencies, e.g., $10\,\mathrm{km}$ offset with $8\,\mathrm{Hz}$. In the shallow water case this zone has a very high error for subsurface resistivities of $1\,\Omega\,\mathrm{m}$ and $10\,\Omega\,\mathrm{m}$ (yellow zones). However, this is due to the fact that the amplitudes of the signal for these offsets and frequencies are in the order of $10^{-25}\,\mathrm{V/m}$.

Another error test is shown in Figure 7. It shows in (a) the amplitude of the analytical fullspace solution for a wide range of resistivities and frequencies: $\rho = 10^{-10}\,\Omega\,\mathrm{m}$ to $10^{10}\,\Omega\,\mathrm{m}$, and $f = 10^{-10}\,\mathrm{Hz}$ to $10^{14}\,\mathrm{Hz}$. In this case, the horizontal offset is set to the skin depth, and the vertical source-receiver separation to a tenth of it, where the skin depth is given by (e.g., Ward and Hohmann, 1988, equation 1.49)

$$z_{\mathrm{skin}} = \left\{ \frac{\omega^2 \varepsilon \mu}{2} \left[ \sqrt{1 + \frac{1}{(\omega \varepsilon \rho)^2}} - 1 \right] \right\}^{-1/2}, \tag{8}$$

where we used in the example $10\,\varepsilon_0$ for the electric permittivity and $\mu_0$ for the magnetic permeability; $\omega = 2\pi f$. The grey contour lines in the figure show the magnitude of the offset: the line with 0 is where the offset is $1\,\mathrm{m}$, the line with 3 where the offset is $1\,\mathrm{km}$, etc. The contour lines of the offset have a knee, after which they become almost independent of

frequency. This is where the quasi static approximation breaks down, and wave phenomena become dominant. The red line indicates where $\omega\varepsilon\rho = 1$. Subplot (b) shows the relative error of the DLF using the filter *Wer201* compared to the analytical solution. It shows nicely that the filter can be used for all cases that are in the quasi static region, but not outside.

We also comment that while it is tempting to design very short length filters (much less than about $N = 100$) since shorter filters can greatly reduce EM simulation times, in our experience, shorter filters tend to be less general purpose than longer filters and we highly recommend thoroughly testing their accuracy for the desired range of data and model parameters.

**Ground-penetrating radar**

Figure 8 shows the GPR example as calculated in Hunziker et al. (2015) and Werthmüller (2017); the model parameters are given in subplot (a). The filter used for this example for the Hankel transform is a 2001 pt filter, derived with the fullspace solution with $f = 500\,\text{MHz}$ for the inversion and the check of quality. The whole space solution used resistivity $200\,\Omega\,\text{m}$, relative permittivity $\varepsilon_{\text{r}} = 10$, and permeability $\mu_{\text{r}} = 1$. Using Equation 8 yields a skin depth of roughly $3.6\,\text{m}$ for these parameters. The source and receiver vertical separation is $1\,\text{m}$. For the Fourier transform a 4096 pt FFT was used with regularly spaced frequencies from $0.5\,\text{MHz}$ to $850\,\text{MHz}$ and then zero-padded up to $2048\,\text{MHz}$. The frequency result is multiplied with a Ricker wavelet with a center frequency of $250\,\text{MHz}$, and a gain function $(1+|t^3|, t$ in ns) is applied. Subplot (b) shows the result when using the adaptive quadrature (QUAD) option of `empymod`, which uses the QAGSE routine from the Fortran QUADPACK

library. Subplot (c) shows the result using DLF with the new 2001 pt digital filter. The calculation with DLF took under 9 minutes and is therefore roughly 80 times faster than the calculation with QUAD, which took roughly 11 hours and 27 minutes. Calculating the same model with QWE took 7 hours and 20 minutes. However, QWE uses in roughly 1/3 of the calculation internally QUAD in this example, see Werthmüller (2017). Note that DLF was run in parallel using 4 threads at once, taking effectively only 2 minutes and 10 seconds to calculate. The lagged convolution version of DLF and the splined version of QWE were used in this comparison.

Figure 9 shows in (a)-(c) the real part of the frequency domain results and in (d)-(f) the time domain results for offsets of 0.2 m, 2.0 m, and 3.0 m.

The 2001 pt filter was derived with the fullspace solution of a medium which is very similar to the layer in which source and receiver reside in our GPR example. To show that this filter can also be applied to different layer parameters we run a test where we swapped layers one and two of the model in Figure 8 (a). The resulting real and imaginary parts for the offsets 0.2 m, 2.0 m, and 3.0 m are given in Figure 10.

These examples show clearly that the filter method can indeed be applied to high frequency EM modeling and therefore wave phenomena. We are convinced that with further tests and analysis much better filters could be achieved, and various concepts could be checked. One approach is to derive a filter for each frequency band, say one for 1 MHz–10 MHz, one for 10 MHz–100 MHz, and one for 100 MHz–1 GHz. Another approach could be to derive distinct filters for $J_0$ and $J_1$, with different spacing and shift values. The first idea would roughly triple the calculation cost, the second idea double them; however, they both would still be very fast compared to standard quadrature methods. One could also

20

apply the digital filter method to acoustic and elastic wavefields as well.

## CONCLUSIONS

The presented, free and open-source code `fdesign` can be used to design digital linear filters for the Hankel and Fourier transforms (and more generally for any linear transform) using either analytical transform pairs or 1D subsurface models together with the EM-modeler `empymod`. The code is available from GitHub ~~in the add-on repository~~ *as part* of `empymod`~~,~~ ~~called~~ ~~`empyscripts`,~~ from version ~~0.2.0~~*1.7.0* onwards.

The presented 201 pt filter achieves more precise results in the three presented CSEM cases than other filters, and is included in `empymod` from version 1.4.5 onwards. However, as with any digital filter, the quality depends heavily on the model, and this new filter might or might not behave that well for other models or data parameters.

The GPR example shows that the digital linear filter method can also be used for wave phenomena, not only for the diffusive approximation limit of low frequency EM modeling.

We see `fdesign` as being useful for at least 3 scenarios:

1. Providing a fast method to design problem-specific filters. For bigger inversion projects (such as, for instance, massive stochastic CSEM inversions) a purpose designed, short filter might save much more time than it costs to design it. This could even be integrated into inversion codes, as an optional pre-inversion step.

2. Extending the filter method to new areas, namely higher frequencies and acoustic and elastic wavefields.

3. Raising interest for digital linear filters in geophysics by making it very easy for anyone

to play around, create their own filters, and get a better understanding of the relative simplicity of the method. We are sure there are many great filters that are yet to be discovered.

## ACKNOWLEDGMENT

# REFERENCES

Anderson, W. L., 1973, Fortran IV programs for the determination of the transient tangential electric field and vertical magnetic field about a vertical magnetic dipole for an m-layer stratified earth by numerical integration and digital linear filtering: USGS, **PB221240**. (https://ntrl.ntis.gov/NTRL/dashboard/searchResults/titleDetail/PB221240.xhtml).

———, 1975, Improved digital filters for evaluating Fourier and Hankel transform integrals: USGS, **PB242800**. (https://pubs.er.usgs.gov/publication/70045426).

———, 1979, Numerical integration of related Hankel transforms of orders 0 and 1 by adaptive digital filtering: Geophysics, **44**, 1287–1305. (doi: 10.1190/1.1441007).

———, 1982, Fast Hankel transforms using related and lagged convolutions: ACM Trans. Math. Softw., **8**, 344–368. (doi: 10.1145/356012.356014).

———, 1984, On: "Numerical integration of related Hankel transforms by quadrature and continued fraction expansion" by Chave (1983): Geophysics, **49**, 1811–1812. (doi: 10.1190/1.1441595).

———, 1989, A hybrid fast Hankel transform algorithm for electromagnetic modeling: Geophysics, **54**, 263–266. (doi: 10.1190/1.1442650).

Bernabini, M., and E. Cardarelli, 1978, The use of filtered Bessel functions in direct interpretation of geoelectrical soundings: Geophysical Prospecting, **26**, 841–852. (doi: 10.1111/j.1365-2478.1978.tb01636.x).

Bichara, M., and J. Lakshmanan, 1976, Fast automatic processing of resistivity soundings*: Geophysical Prospecting, **24**, 354–370. (doi: 10.1111/j.1365-2478.1976.tb00932.x).

Chave, A. D., 1983, Numerical integration of related Hankel transforms by quadrature and continued fraction expansion: Geophysics, **48**, 1671–1686. (doi: 10.1190/1.1441448).

Christensen, N. B., 1990, Optimized fast Hankel transform filters: Geophysical Prospecting,

**38**, 545–568. (doi: 10.1111/j.1365-2478.1990.tb01861.x).

Das, U. C., 1982, Designing digital linear filters for computing resistivity and electromagnetic sounding curves: Geophysics, **47**, 1456–1459. (doi: 10.1190/1.1441295).

———, 1984, A single digital linear filter for computations in electrical methods–a unifying approach: Geophysics, **49**, 1115–1118. (doi: 10.1190/1.1441726).

Das, U. C., and D. P. Ghosh, 1974, The determination of filter coefficients for the computation of standard curves for dipole resistivity sounding over layered earth by linear digital filtering: Geophysical Prospecting, **22**, 765–780. (doi: 10.1111/j.1365-2478.1974.tb00117.x).

Das, U. C., D. P. Ghosh, and D. T. Biewinga, 1974, Transformation of dipole resistivity sounding measurements over layered earth by linear digital filtering: Geophysical Prospecting, **22**, 476–489. (doi: 10.1111/j.1365-2478.1974.tb00100.x).

Das, U. C., and S. K. Verma, 1980, Digital linear filter for computing type curves for the two-electrode system of resistivity sounding: Geophysical Prospecting, **28**, 610–619. (doi: 10.1111/j.1365-2478.1980.tb01246.x).

———, 1981a, Numerical considerations on computing the EM response of three-dimensional inhomogeneities in a layered earth: Geophysical Journal International, **66**, 733–740. (doi: 10.1111/j.1365-246X.1981.tb04897.x).

———, 1981b, The versatility of digital linear filters used in computing resistivity and em sounding curves: Geoexploration, **18**, 297–310. (doi: 10.1016/0016-7142(81)90059-4).

———, 1982, Electromagnetic response of an arbitrarily shaped three-dimensional conductor in a layered earth — numerical results: Geophysical Journal International, **69**, 55–66. (doi: 10.1111/j.1365-246X.1982.tb04935.x).

Davis, P. A., S. A. Greenhalgh, and N. P. Merrick, 1980, Resistivity sounding computations

with any array using a single digital filter: Exploration Geophysics, **11**, 54–62. (doi: 10.1071/EG980054).

Ghosh, D. P., 1970, The application of linear filter theory to the direct interpretation of geoelectrical resistivity measurements: Ph.D. Thesis, TU Delft. (uuid: 88a568bb-ebee-4d7b-92df-6639b42da2b2).

———, 1971a, The application of linear filter theory to the direct interpretation of geoelectrical resistivity sounding measurements: Geophysical Prospecting, **19**, 192–217. (doi: 10.1111/j.1365-2478.1971.tb00593.x).

———, 1971b, Inverse filter coefficients for the computation of apparent resistivity standard curves for a horizontally stratified earth: Geophysical Prospecting, **19**, 769–775. (doi: 10.1111/j.1365-2478.1971.tb00915.x).

Guptasarma, D., 1982, Optimization of short digital linear filters for increased accuracy: Geophysical Prospecting, **30**, 501–514. (doi: 10.1111/j.1365-2478.1982.tb01320.x).

Guptasarma, D., and B. Singh, 1997, New digital linear filters for Hankel J0 and J1 transforms: Geophysical Prospecting, **45**, 745–762. (doi: 10.1046/10.1046/j.1365-2478.1997.500292.x).

Hunziker, J., J. Thorbecke, and E. Slob, 2015, The electromagnetic response in a layered vertical transverse isotropic medium: A new look at an old problem: Geophysics, **80**, no. 1, F1–F18. (doi: 10.1190/geo2013-0411.1).

Johansen, H. K., 1975, An interactive computer/graphic-display-terminal system for interpretation of resistivity soundings: Geophysical Prospecting, **23**, 449–458. (doi: 10.1111/j.1365-2478.1975.tb01541.x).

Johansen, H. K., and K. Sørensen, 1979, Fast Hankel transforms: Geophysical Prospecting, **27**, 876–901. (doi: 10.1111/j.1365-2478.1979.tb01005.x).

Key, K., 2009, 1D inversion of multicomponent, multifrequency marine CSEM data: Methodology and synthetic studies for resolving thin resistive layers: Geophysics, **74**, no. 2, F9–F20. (doi: 10.1190/1.3058434).

——, 2012, Is the fast Hankel transform faster than quadrature?: Geophysics, **77**, no. 3, F21–F30. (doi: 10.1190/GEO2011-0237.1).

Koefoed, O., 1968, The application of the kernel function in interpreting geoelectrical resistivity measurements: Gebrüder Borntraeger. (ISBN: 9783443130022).

——, 1970, A fast method for determining the layer distribution from the raised kernel function in geoelectrical sounding: Geophysical Prospecting, **18**, 564–570. (doi: 10.1111/j.1365-2478.1970.tb02129.x).

——, 1972, A note on the linear filter method of interpreting resistivity sounding data: Geophysical Prospecting, **20**, 403–405. (doi: 10.1111/j.1365-2478.1972.tb00643.x).

——, 1976, Error propagation and uncertainty in the interpretation of resistivity sounding data: Geophysical Prospecting, **24**, 31–48. (doi: 10.1111/j.1365-2478.1976.tb00383.x).

Koefoed, O., and F. J. H. Dirks, 1979, Determination of resistivity sounding filters by the Wiener-Hopf least-squares method: Geophysical Prospecting, **27**, 245–250. (doi: 10.1111/j.1365-2478.1979.tb00968.x).

Koefoed, O., D. P. Ghosh, and G. J. Polman, 1972, Computation of type curves for electromagnetic depth sounding with a horizontal transmitting coil by means of a digital linear filter: Geophysical Prospecting, **20**, 406–420. (doi: 10.1111/j.1365-2478.1972.tb00644.x).

Kong, F. N., 2007, Hankel transform filters for dipole antenna radiation in a conductive medium: Geophysical Prospecting, **55**, 83–89. (doi: 10.1111/j.1365-2478.2006.00585.x).

Kruglyakov, M., and L. Bloshanskaya, 2017, High-performance parallel solver for integral equations of electromagnetics based on Galerkin method: Mathematical Geosciences, **49**,

751–776. (doi: 10.1007/s11004-017-9677-y).

Kumar, R., and U. C. Das, 1977, Transformation of dipole to Schlumberger sounding curves by means of digital linear filters: Geophysical Prospecting, **25**, 780–789. (doi: 10.1111/j.1365-2478.1977.tb01204.x).

———, 1978, Transformation of Schlumberger apparent resistivity to dipole apparent resistivity over layered earth by the application of digital linear filters: Geophysical Prospecting, **26**, 352–358. (doi: 10.1111/j.1365-2478.1978.tb01598.x).

Mohsen, A. A., and E. A. Hashish, 1994, The fast Hankel transform: Geophysical Prospecting, **42**, 131–139. (doi: 10.1111/j.1365-2478.1994.tb00202.x).

Murakami, Y., and T. Uchida, 1982, Accuracy of the linear filter coefficients determined by the iteration of the least-squares method: Geophysics, **47**, 244–256. (doi: 10.1190/1.1441331).

Newman, G. A., G. W. Hohmann, and W. L. Anderson, 1986, Transient electromagnetic response of a three-dimensional body in a layered earth: Geophysics, **51**, 1608–1627. (doi: 10.1190/1.1442212).

Nissen, J., and T. Enmark, 1986, An optimized digital filter for the Fourier transform: Geophysical Prospecting, **34**, 897–903. (doi: 10.1111/j.1365-2478.1986.tb00500.x).

Niwas, S., 1975, Direct interpretation of geoelectric measurements by the use of linear filter theory: Geophysics, **40**, 121–122. (doi: 10.1190/1.1440510).

Nyman, D. C., and M. Landisman, 1977, VES dipole-dipole filter coefficients: Geophysics, **42**, 1037–1044. (doi: 10.1190/1.1440763).

O'Neill, D., 1975, Improved linear filter coefficients for application in apparent resistivity computations: Exploration Geophysics, **6**, 104–109. (doi: 10.1071/EG975104).

O'Neill, D. J., and N. P. Merrick, 1984, A digital linear filter for resistivity sounding with a

generalized electrode array: Geophysical Prospecting, **32**, 105–123. (doi: 10.1111/j.1365-2478.1984.tb00720.x).

Pekeris, C. L., 1940, Direct method of interpretation in resistivity prospecting: Geophysics, **5**, 31–42. (doi: 10.1190/1.1441791).

Raiche, A., F. Sugeng, and G. Wilson, 2007, Practical 3D EM inversion - the P223F software suite: ASEG Technical Program Expanded Abstracts, 1–4. (doi: 10.1071/ASEG2007ab114).

Slichter, L. B., 1933, The interpretation of the resistivity prospecting method for horizontal structures: Physics, **4**, 307–322. (doi : 10.1063/1.1745198).

Sørensen, K. I., and N. B. Christensen, 1994, The fields from a finite electrical dipole—a new computational approach: Geophysics, **59**, 864–880. (10.1190/1.1443646).

Verma, R. K., and O. Koefoed, 1973, A note on the linear filter method of computing electromagnetic sounding curves: Geophysical Prospecting, **21**, 70–76. (doi: 10.1111/j.1365-2478.1973.tb00015.x).

Ward, S. H., and G. W. Hohmann, 1988, Electromagnetic theory for geophysical applications: SEG, Investigations in Geophysics, No. 3, 4, 130–131. (doi: 10.1190/1.9781560802631).

Werthmüller, D., 2017, An open-source full 3D electromagnetic modeler for 1D VTI media in Python: empymod: Geophysics, **82**, no. 6, WB9–WB19. (doi: 10.1190/geo2016-0626.1).

# LIST OF FIGURES

(yellow zones). However, the amplitudes in these regions are in the order of $10^{-25}$ V/m, and therefore far below the noise level.

7    (a) Amplitude of the analytical fullspace solution for a wide range of resistivities and frequencies. The contour lines show the power of the offset used for the calculation, where the offset is set to the skin depth. (b) Relative error of the DLF compared with the analytical solution. The filter *Wer201* works well in the diffusive limit, but fails when wave phenomena become dominant. The red line shows where $\omega\varepsilon\rho = 1$.

8    GPR example for the model given in (a) using `empymod` with (b) the adaptive quadrature (QUAD) or with (c) a 2001 pt digital linear filter (b). QUAD took about 11 h 27 min to calculate, whereas DLF took 2 min 10 s in parallel on 4 nodes, hence under 9 min in total.

9    The real-part frequency-domain and the time-domain responses for offsets of (a/d) 0.2 m, (b/e) 2.0 m, and (c/f) 3.0 m.

10    The real and imaginary parts of the frequency-domain response for the model given in Figure 8 (a) with swapped first and second layers for offsets of (a) 0.2 m, (b) 2.0 m, and (c) 3.0 m.
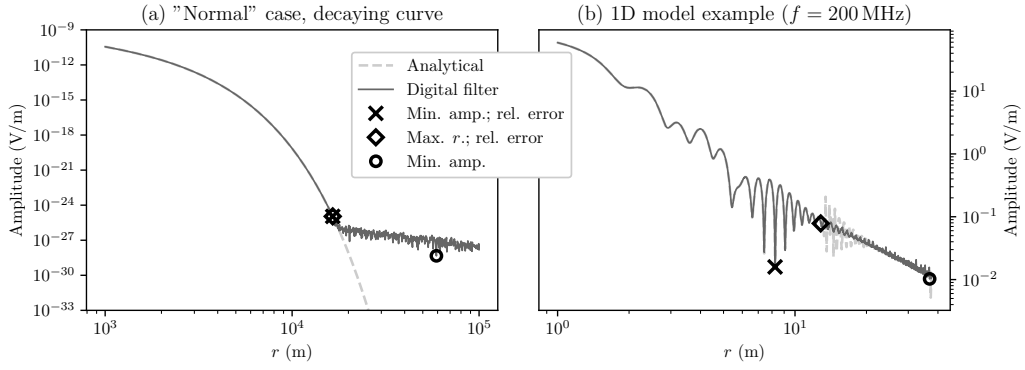
Figure 1: (a) A regular RHS curve of a transform pair with a purely decaying function. Minimum amplitude or maximum $r$ yield the same result in this scenario. Using a relative error criteria is more stable than just the absolute minimum amplitude. (b) A 1D model for $f = 200\,\mathrm{MHz}$. Here, the maximum $r$ provides a better criteria for the inversion.
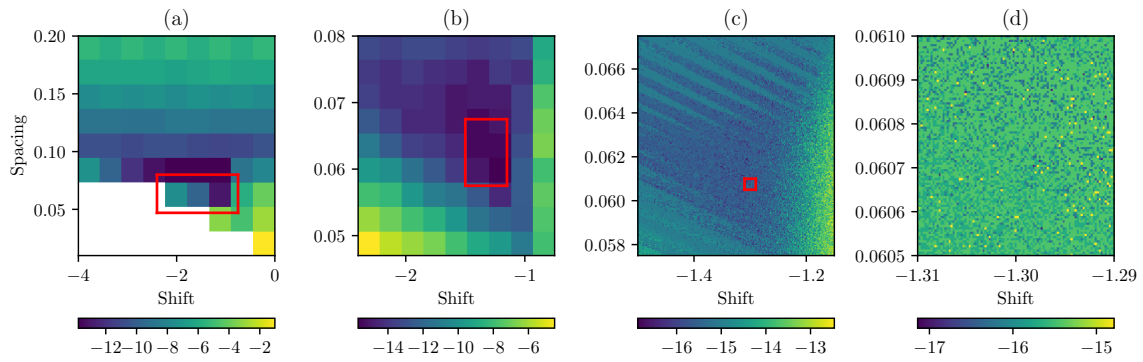
– **GEO-2018-0069.R2**

Figure 2: Solution spaces of four consecutive inversion runs for a 201 pt filter. Each consecutive run zooms into a portion of the previous solution space, indicated by the red square. The more in detail we obtain the solution space, the more random appears to be the distribution.

– **GEO-2018-0069.R2**
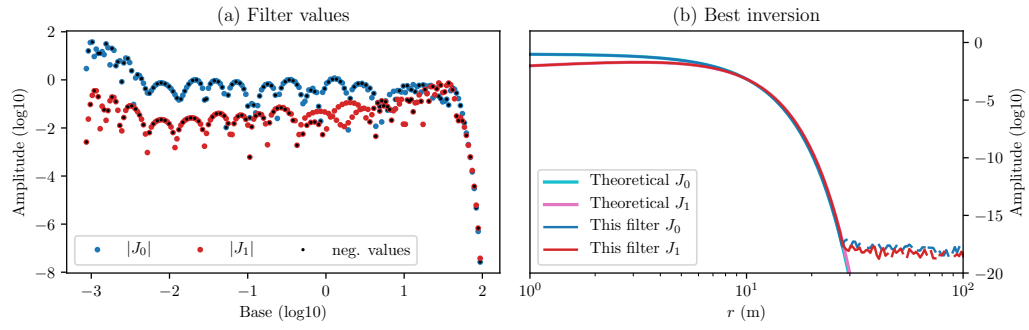
Figure 3: (a) Filter values of the best obtained 201 pt filter with the corresponding check of quality in (b). Black points indicate negative values, which shows that adjacent values have often opposite signs.

– **GEO-2018-0069.R2**
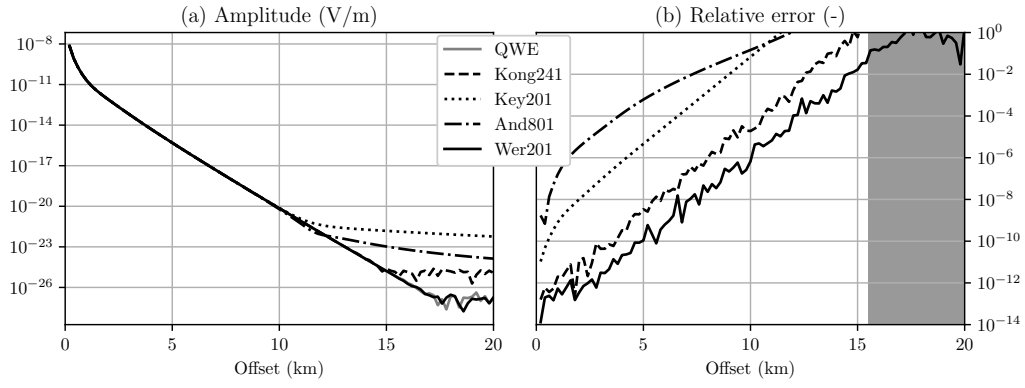
Figure 4: (a) Results of different filters and QWE for the model of Figure 5 from Kong (2007) with the relative errors shown in (b), using the QWE result. The relative error is meaningless from about 15.5 km onwards, as QWE failed as well for these very low amplitudes.

– **GEO-2018-0069.R2**
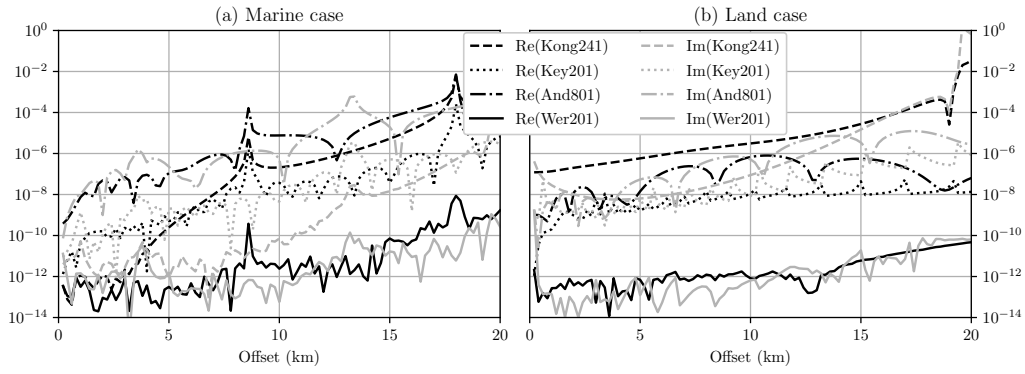
Figure 5: (a) The canonical marine CSEM model of Key (2012) and (b) a land model with source and receiver at the surface. The new filter has generally relative errors which are several orders of magnitude lower than the other filters.
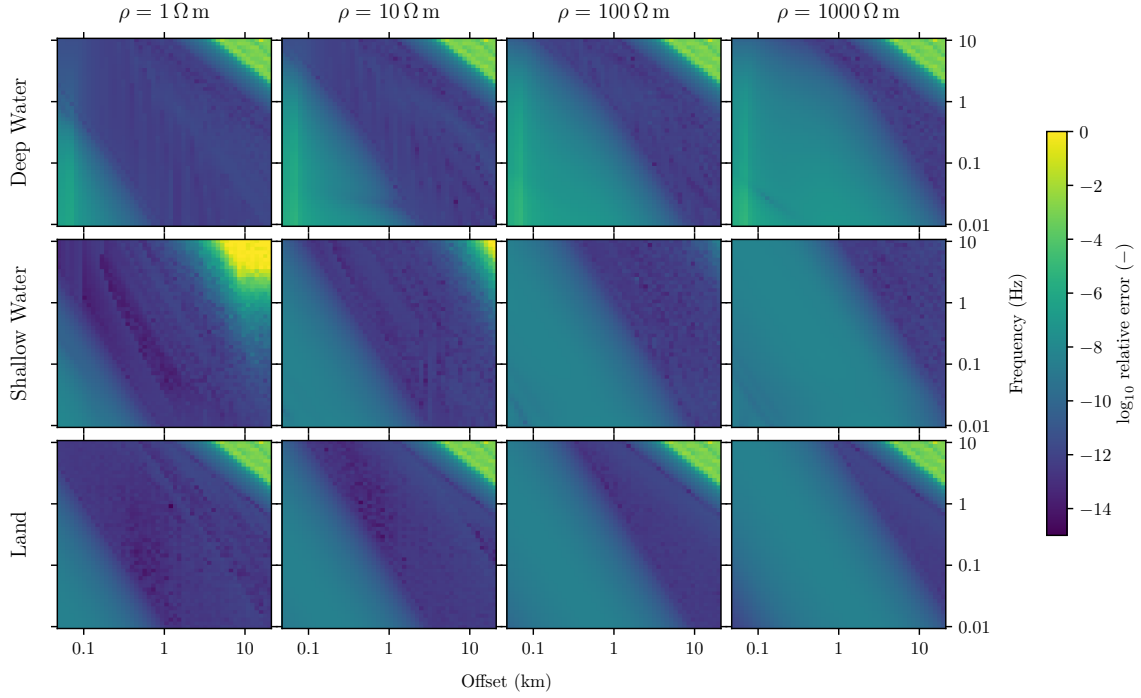
– **GEO-2018-0069.R2**

Figure 6: Relative error plots comparing the DLF (*Wer201*) with QWE for the three cases deep water (top row), shallow water (middle row), and land (bottom row). The subsurface halfspace resistivity varies from 1 to $1000\,\Omega\,\mathrm{m}$ from the left column to the right column; offsets vary from $50\,\mathrm{m}$ to $20\,\mathrm{km}$, and frequencies vary from $0.01\,\mathrm{Hz}$ to $10\,\mathrm{Hz}$. The DLF provides sufficiently accurate results for all practical CSEM applications. The exception is in the shallow water case for $\rho = 1\,\Omega\,\mathrm{m}$ and $10\,\Omega\,\mathrm{m}$ for large offsets and high frequencies (yellow zones). However, the amplitudes in these regions are in the order of $10^{-25}\,\mathrm{V/m}$, and therefore far below the noise level.
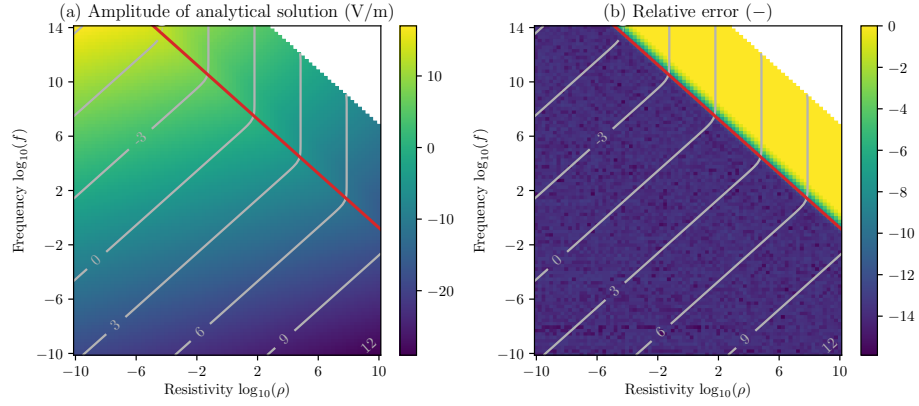
– **GEO-2018-0069.R2**

Figure 7: (a) Amplitude of the analytical fullspace solution for a wide range of resistivities and frequencies. The contour lines show the power of the offset used for the calculation, where the offset is set to the skin depth. (b) Relative error of the DLF compared with the analytical solution. The filter *Wer201* works well in the diffusive limit, but fails when wave phenomena become dominant. The red line shows where $\omega\varepsilon\rho = 1$.
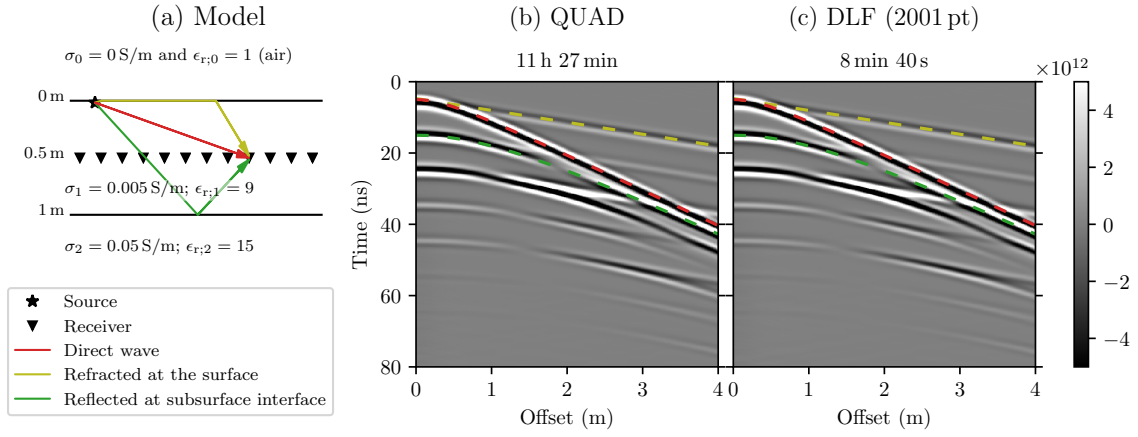
– **GEO-2018-0069.R2**

Figure 8: GPR example for the model given in (a) using `empymod` with (b) the adaptive quadrature (QUAD) or with (c) a 2001 pt digital linear filter (b). QUAD took about 11 h 27 min to calculate, whereas DLF took 2 min 10 s in parallel on 4 nodes, hence under 9 min in total.
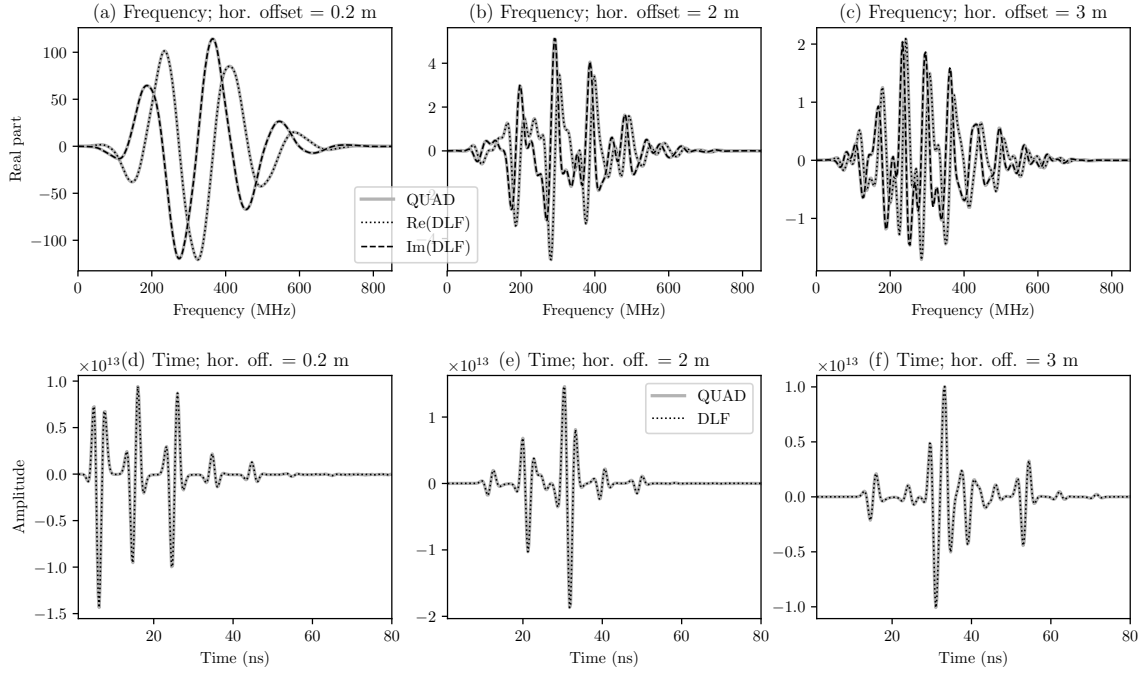
– **GEO-2018-0069.R2**

Figure 9: The real-part frequency-domain and the time-domain responses for offsets of (a/d) 0.2 m, (b/e) 2.0 m, and (c/f) 3.0 m.
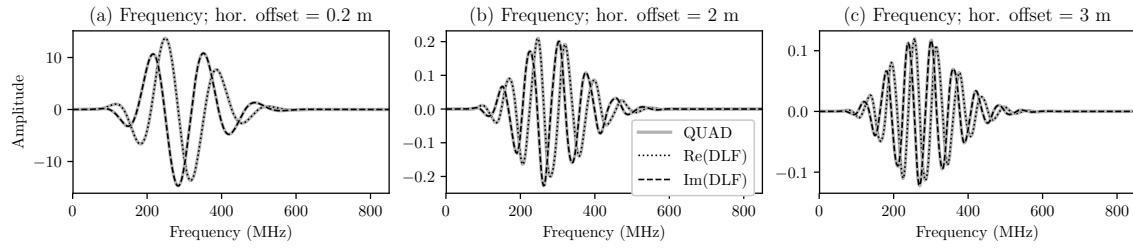
– **GEO-2018-0069.R2**

Figure 10: The real and imaginary parts of the frequency-domain response for the model given in Figure 8 (a) with swapped first and second layers for offsets of (a) 0.2 m, (b) 2.0 m, and (c) 3.0 m.

– **GEO-2018-0069.R2**